Published in final edited form as:
Magn Reson Med. 2013 March 1; 69(3): 675–681. doi:10.1002/mrm.24295.

Test-retest reproducibility of a rapid method to measure brain oxygen metabolism

Peiying Liu[1], **Feng Xu**[1], and **Hanzhang Lu**[1,*]

[1]Advanced Imaging Research Center, University of Texas Southwestern Medical Center, Dallas, Texas, United States

Abstract

Cerebral metabolic rate of oxygen ($CMRO_2$) is an important index of tissue viability and brain function, but this parameter cannot yet be measured routinely on clinical scanners. Recently, a non-invasive technique was proposed which estimates global $CMRO_2$ by concomitantly measuring Oxygen-Extraction-Fraction (OEF) using T_2-Relaxation-Under-Spin-Tagging (TRUST) MRI and pulse oximetry, and Cerebral-Blood-Flow (CBF) using phase-contrast MRI. The present study sought to establish a standard acquisition procedure for this technique and to evaluate its test-retest reproducibility in healthy subjects. Each subject was examined in five sessions and each session included two measurements. Intra-session, inter-session, and inter-subject coefficients of variation (CoV) for $CMRO_2$ were found to be 3.84±1.44% (N=7, mean ± standard deviation), 6.59 ± 1.56%, and 8.80% respectively. These reproducibility values were comparable or slightly superior to ^{15}O PET results reported in the literature. It was also found that OEF and CBF tended to co-vary across sessions (p=0.002) and subjects (p=0.01), and their CoVs were greater than that of $CMRO_2$. The simplicity and reliability features may afford this global $CMRO_2$ technique great potential for immediate clinical applications.

Keywords

cerebral metabolic rate of oxygen; cerebral blood flow; venous oxygenation; oxygen extraction fraction

Introduction

Cerebral metabolic rate of oxygen ($CMRO_2$) refers to the amount of oxygen consumed by the brain per unit time, and is often written in units of ml O_2 per 100 g tissue per minute. Because oxidative metabolism is the primary means of energy production in the brain (1), $CMRO_2$ is an important index of tissue viability and brain health. Abnormal levels of $CMRO_2$ have been reported in a number of conditions such as Alzheimer's disease (2–3), brain aging (4), multiple sclerosis (5–6), Parkinson's disease (7), diabetes (8–9), traumatic brain injury (10), and normal pressure hydrocephalus (11). Therefore, a non-invasive, fast, and reliable method to quantify $CMRO_2$ is expected to have immediate impact in many clinical conditions.

Currently established methods for $CMRO_2$ measurement usually require the use of exogenous tracer (e.g., $^{15}O_2$ in PET (12–15), $^{17}O_2$ in NMR (16), N_2O in Kety-Schmidt method (17–18), and ^{13}C in NMR (19)), continuous blood sampling, and special equipment

*Corresponding Author: Hanzhang Lu, Ph.D. Advanced Imaging Research Center UT Southwestern Medical Center 5323 Harry Hines Blvd. Dallas, TX 75390 hanzhang.lu@utsouthwestern.edu Tel: 214-645-2761 Fax: 214-645-2744.

(e.g. cyclotron). These complexities in experimental procedures in combination with the relatively high costs have prohibited $CMRO_2$ from becoming a routine clinical measure. More recently, a number of newer technologies have been proposed for the measurement of $CMRO_2$ without using exogenous tracers (20–32). Calibrated fMRI uses purely vascular challenges to obtain an estimation of $CMRO_2$ percentage change associated with neural activation (24–27) and, when multiple physiologic challenges (e.g. hypercapnia and hyperoxia) are applied concomitantly, absolute $CMRO_2$ values may also be calculated (28). Other methods have used extravascular BOLD effect (29), phase angle of venous blood (30), and optical properties of venous blood (31–32) to estimate $CMRO_2$.

Our laboratory has recently devised an MR method to estimate whole-brain $CMRO_2$ by combining non-invasive measurements of cerebral blood flow (CBF), arterial and venous oxygenation (21). In this method, whole brain CBF was measured by phase-contrast (PC) MRI (33) while arterial oxygenation (Y_a) was measured by pulse oximetry. The most challenging component, venous oxygenation (Y_v), was measured by a T_2-Relaxation-Under-Spin-Tagging (TRUST) MRI technique that was developed in our laboratory (34). Global $CMRO_2$ is calculated from these parameters using the Fick principle of arteriovenous difference (17). Despite the lack of spatial information, several desirable features of this method, e.g. non-invasiveness (no exogenous agent), fast (about 3–7 min in scan time), availability on a standard clinical scanner, allowed an easy application of the technique in several physiologic and clinical studies (4–5,35–37). These preliminary evidences demonstrated a great potential for this measure to serve as a biomarker in several neurological conditions. However, in order for this method to be widely used by the clinical community, a standard acquisition procedure as well as the test-retest reproducibility needs to be established.

Therefore, the purpose of the present study is to describe a standard protocol for non-invasive evaluation of $CMRO_2$ and to test the reliability of this method. While Xu et al. (21) have shown a proof-of-principle of this design, the proposed protocol incorporated the more recent advances in the TRUST technique which allowed us to reduce the scan duration by 63% while maintaining measurement accuracy (38). The phase-contrast measurement has also been adjusted to better reflect global CBF. We studied seven healthy subjects and each subject was examined for five times on different days. Within each session, the scans were repeated once. These data allowed us to evaluate the intra-session and inter-session reproducibility as well as inter-subject variations of CBF, Y_v, OEF and $CMRO_2$ measurements.

Materials and Methods

Framework of the $CMRO_2$ measurement

The theoretical basis of our $CMRO_2$ measurement is the Fick Principle of arteriovenous oxygen difference, a principle used by Kety and Schmidt in their original $CMRO_2$ measurement (17). Brain oxygen metabolic rate is given by:

$$CMRO_2 = CBF \cdot (Y_a - Y_v) \cdot C_a \quad [1]$$

where CBF is the whole-brain blood flow in ml/100 g/min, Y_a and Y_v are oxygen saturation fraction in arterial and venous blood in %, respectively; and C_a is the amount of oxygen molecules that a unit volume of blood can carry and is well established in physiology literature (897 μmol O_2/100 ml blood for hematocrit level of 0.44) (39). Some researchers further define a term called oxygen extraction fraction (OEF), given by OEF = $(Y_a\text{-}Y_v)/Y_a \times 100\%$.

Y_v is determined using a recently developed and validated TRUST MRI technique (34,40). Briefly, TRUST MRI utilizes the spin-tagging principle on the venous side to separate out the pure venous blood signal by subtracting the labeled image from the control image. The label and control scans are performed with various numbers of flow-insensitive T_2-preparation pulses to modulate the signal with different T_2 weightings. The monoexponential fitting of the blood signal to the T_2-preparation duration (termed effective TE [eTE]) then gives the T_2 value of the venous blood. Since blood T_2 has a well-known relationship with the oxygenation level of the blood, the estimated venous T_2 can be converted to Y_v via a calibration plot obtained by a set of *in vitro* experiments (40).

Global CBF is measured by a phase-contrast (PC) quantitative flow technique (33) applied at the feeding arteries at the base of the brain. Phase-contrast MRI utilizes the phase of an image to encode the velocity of moving spins and has been validated for angiogram and quantitative flow measurements (41–43).

Y_a is relatively homogenous across individuals. One can use literature values (e.g. 98%) or can measure this parameter non-invasively on the finger tip with pulse oximetry.

Proposed protocol for $CMRO_2$ measurement

In this section, we provide detailed steps to obtain a complete $CMRO_2$ dataset, so that readers can feasibly reproduce these procedures (Fig. 1).

The measurement started with an axial 3D time-of-flight (TOF) angiogram for which the top of the slab is at the level of the bottom of pons (Fig. 2a). This allowed the operator to visualize the feeding arteries of the brain which is necessary for PC MRI slice positioning (Fig. 2b). The imaging parameters of the TOF angiogram were: TR/TE/flip angle = 20 ms/3.45 ms/18°, FOV = 160 × 160 × 70.5 mm^3, voxel size = 1.0 × 1.0 × 1.5 mm^3, number of slices = 47, one 60 mm saturation slab positioned above the imaging slab, scan duration = 1.4 min.

After TOF angiogram, a TRUST scan was performed. The imaging slice was positioned to be parallel to anterior-commissure posterior-commissure line with a distance of 20 mm from the sinus congruence where the superior sagittal sinus (SSS), straight sinus and transverse sinus join (Fig. 2d). This empirical criterion allowed the imaging slice to intersect SSS at an angle close to 90°. A post-sat TRUST sequence (38) was used with the following parameters: TR = 3000 ms, TI = 1200 ms, voxel size = 3.44 × 3.44 × 5 mm^3, four different T_2-weightings with eTEs of 0 ms, 40 ms, 80 ms and 160 ms, with a τ_{CPMG} = 10 ms, scan duration = 1.2 min. The labeling slab was 100 mm in thickness and was positioned 22.5 mm above the imaging slice. This allows sufficient labeling of venous blood in upstream vessels.

While the TRUST scan was being performed, the operator planned the PC MRI scans. Based on the maximum intensity projection (MIP) images from the TOF angiogram, four PC MRI scans were planned corresponding to the four feeding arteries of the brain, left internal carotid artery (left ICA), right internal carotid artery (right ICA), left vertebral artery (left VA) and right vertebral artery (right VA), respectively (Fig. 2b). Ideally, the PC MRI slices should be placed at the level of foramen magnum where the arteries enter the skull (green dashed line in Fig. 2b). This was feasible for ICAs which do not make obvious turns in this region. For VAs, however, this was found to be difficult in practice due to complexity in vascular trajectory at this level. Therefore, the positions for VA PC MRI were chosen to be the mid point of an immediately lower segment (parentheses in Fig. 2b) of the arteries, which are slightly below foramen magnum. More discussions on the positioning of PC MRI and comparison to the previous study (21) are given in Discussion section. For all PC MRI scans, the center of the FOV was placed to overlap with the center of the targeted artery.

This procedure allowed an easy identification of the proper artery during post-processing, which is useful in practice as there are a considerable number of blood vessels in the neck region. Imaging parameters of PC MRI are: single slice, voxel size = 0.45 × 0.45 × 5 mm^3, FOV = 230 × 230 × 5 mm^3, maximum velocity encoding = 80 cm/s, 4 averages, scan duration of one PC MRI scan is 0.5 min.

The total duration to obtain a $CMRO_2$ dataset is approximately 5 minutes.

Reproducibility study

Seven healthy subjects (3 males, 4 females, age 26.4 ± 4.0 years) participated in the study. All MRI experiments were performed on a 3T MRI scanner (Achieva, Philips Medical Systems, The Netherlands) using a body coil for RF transmission and an eight-channel sensitivity encoding head coil for receiving. Foam padding was used to stabilize the head and minimize motion. The protocol was approved by University of Texas Southwestern Medical Center's Institutional Review Board and informed written consent was obtained from each participant.

Each subject was scanned on 5 separate sessions within a 13 day period, with a minimum gap of 1 day. During each session, the above-described $CMRO_2$ procedure was performed twice with a 12 min gap but without repositioning of the subject. In addition, a T_1-weighted magnetization-prepared rapid gradient-echo (MPRAGE) image (voxel size = 1 × 1 × 1 mm^3) was acquired in the first session of each subject to provide an estimation of the brain volume, so that variances in brain sizes can be accounted for when comparing $CMRO_2$ across subjects. Note that an anatomic scan is acquired in virtually all studies, thus this scan time was not included when calculating the time needed to obtain a $CMRO_2$ dataset. The arterial oxygen saturation fraction (Y_a, in %) was also measured once only (with a pulse oximetry device made by Invivo, Gainesville, FL) because Y_a is known to be relatively stable and its influence on $CMRO_2$ is expected to be small compared to the other experimental measures (4).

Data analysis

Data processing of TRUST and PC MRI followed methods used previously (21,34,40). Briefly, for TRUST MRI data, after motion correction and pair-wise subtraction between control and tag images, a preliminary region-of-interest (ROI) was manually drawn to include the superior sagittal sinus. To further define the venous voxels, four voxels with the highest signals in the difference images in the ROI were chosen as the final mask for spatial averaging. The venous blood signals were then fitted to a monoexponential function to obtain T_2. The T_2 was in turn converted to Y_v via a calibration plot obtained by *in vitro* bovine blood experiments under controlled oxygenation, temperature, and Hct conditions (40). For PC MRI data, a ROI was manually drawn on the targeted artery of each PC MRI scans based on the magnitude image. The operator was instructed to trace the boundary of the targeted artery without including adjacent vessels. The phase signals, i.e. velocity values, within the mask were summed to yield the blood flow of each artery. To account for brain size differences, the unit volume CBF (in ml/100 g/min) was obtained by normalizing the total CBF (in ml/min) of all four arteries to the intracranial mass (in gram), which was estimated from the high resolution T_1-MPRAGE image using the software FSL (FMRIB Software Library, Oxford University). OEF was calculated from Y_a and Y_v.

Several reproducibility indices were calculated for each of the physiologic parameters evaluated. Intra-session Coefficient of Variation (CoV) was calculated as:

$$CoV_{\text{intra-session}} = \frac{1}{I \cdot J} \sum_i \sum_j \frac{|M_{ij1} - M_{ij2}|}{\sqrt{2} \cdot Mean\left(M_{ij1}, M_{ij2}\right)} \quad (2)$$

where M_{ij1} and M_{ij2} represent measurement #1 and #2, respectively of Subject #i (i = 1, 2, …, I) in Session #j (j = 1, 2, …, J). Inter-session CoV was calculated as:

$$CoV_{\text{inter-session}} = \frac{1}{I \cdot K} \sum_i \sum_k \frac{SD_j\left(M_{ijk}\right)}{Mean_j\left(M_{ijk}\right)} \quad (3)$$

where SD stands for standard deviation.

Inter-subject CoV was calculated as:

$$CoV_{\text{inter-subject}} = \frac{1}{I \cdot K} \sum_j \sum_k \frac{SD_i\left(M_{ijk}\right)}{Mean_i\left(M_{ijk}\right)} \quad (4)$$

Compared to intra-session CoV, the value of inter-session is expected to contain additional variance due to subject repositioning and day-to-day differences in physiologic states. These contributions can be calculated as $\sqrt{CoV^2_{\text{inter-session}} - CoV^2_{\text{intra-session}}}$. Similarly, compared to inter-session CoV, inter-subject CoV contains additional inter-subject physiologic differences. These contributions can be calculated as $\sqrt{CoV^2_{\text{inter-subject}} - CoV^2_{\text{inter-session}}}$.

Additionally, since CBF quantification involves manual ROI selection, inter-rater reliability of CBF measurement was evaluated by having two raters (PL and FX) analyze the same datasets independently and calculating the correlation of the CBF values.

Relationships between physiologic parameters were evaluated with Pearson correlation and mixed effect model. In all analyses, a $p < 0.05$ is considered statistically significant.

Results

All subjects successfully completed all sessions. Representative PC and TRUST MR images are shown in Fig. 2c and e, respectively. Table 1 summarizes the average values and the intra-session, inter-session, and inter-subject CoV for Y_v, OEF, CBF, and $CMRO_2$. It can be seen that the intra-session CoV, which reflects the measurement noise, is less than 4% for all parameters, suggesting high reliability of the techniques used. Figs. 3a and 3b show a Bland-Altman plot and a scatter plot, respectively, between two $CMRO_2$ measurements in the same session, again demonstrating a strong consistency across measurements ($r = 0.67$, $p < 0.001$).

Inter-session CoV was higher than intra-session CoV (Table 1), as addition sources of variance are included. The subject repositioning and day-to-day physiologic fluctuations, as calculated by the root square difference between inter- and intra-session CoV, were estimated to be 5.35% for $CMRO_2$ measurements.

Inter-subject CoV was 8.8% (Table 1). It is interesting to note that inter-subject variations in CBF and OEF were much greater ($p<0.001$) than that of their product, $CMRO_2$. This is because CBF and OEF co-vary across individuals, as can be seen in their scatter plot (Fig. 4, $p = 0.01$). That is, an individual with a higher CBF tends to have a lower OEF, thus their

effects partly cancel out in the $CMRO_2$. In fact, the same statement can be made for measurements across sessions (see dots with the same colors in Fig. 4, mixed effect model $p = 0.002$). That is, if a subject shows a higher CBF in a session, his OEF in this session will tend to be lower.

For CBF processing which involves manual ROI drawing, we observed a high inter-rater reliability of $r = 0.997$ and $p < 0.0001$ (fitting line y = 1.002×).

Discussion

The $CMRO_2$ method under investigation, originally proposed by Xu et al (21), has great potentials in understanding brain physiology and brain diseases (4–5,35–37). Compared to the few existing $CMRO_2$ methods including ^{15}O PET (12–15), ^{13}C NMR (19), and ^{17}O NMR (16), this method has the advantages of being non-invasive (no exogenous agent needed), rapid (<5 min in scan time), and can be implemented on a standard clinical scanner. Critical but missing steps are the establishment of a standard acquisition procedure and a thorough investigation of test-retest reproducibility. The present study intends to fill these gaps. Here we provide step-by-step instructions on the orders of the necessary scans with details on slice positioning. The performance of this procedure was tested extensively from the data in the present study as well as other ongoing studies in our laboratory. While all previous test-retest studies on $CMRO_2$ have only attempted two sessions (12–13,16,27), we conducted a five-session reproducibility evaluation and showed that global $CMRO_2$ measured with this method has an intra-session, inter-session, and inter-subject CoV of 4%, 7%, and 9%, respectively. These data provide an important reference for future studies when deciding whether this method can be applied or when conducting power calculations.

The intra-session CoV of the present technique (Table 1) was slightly lower than those reported for ^{15}O PET, which was found to be 5.7 ± 4.4%, 8.4 ± 7.6%, and 5.3 ± 3.9% for OEF, CBF and $CMRO_2$, respectively (13). For inter-session CoV, the values obtained in this study was comparable to the PET reports, which were 9.3%, 8.8%, and 5.3% for OEF, CBF, and $CMRO_2$, respectively (12). The inter-subject CoV in the present study is also in good agreement with that in the PET studies, which ranged from 7.1–12.8% (12–13). Compared to CBF measurements with Arterial-Spin-Labeling (ASL) techniques, which showed an intra-session CoV of 3.5–7.5% and an inter-session CoV of 8.5–16.6% (44), the PC MRI technique used in the present study showed a smaller variation, presumably because ASL MRI contains a few confounding factors associated with labeling efficiency, arterial transit time, and T_1 relaxation (45–46). It should be mentioned that several other non-invasive $CMRO_2$ methods have been proposed recently. These methods were based on susceptibility effect in extravascular tissue (20,29), phase angle in intravascular blood signal (30), and T_2 value of regional blood signal (47). A full assessment of test-retest reproducibility of these methods has not been reported and should be investigated in future studies.

Compared to the procedure used in the original report of this technique (21), the proposed protocol have made the following changes/improvements. For the estimation of Y_v, Xu et al. have recently proposed a modified TRUST sequence in which a non-selective saturation RF pulse was applied immediately after image acquisition to reset the magnetizations of all spins (38). When combined with an optimal TR and TE, this sequence was found to reduce the scan duration by 63% while maintaining estimating accuracy and precision (38). This improvement in TRUST technique has been adopted in the present study. For PC MRI, the previous report applied the imaging slice at the level of cervical spinal cord 3 (C3), where all four arteries (left/right ICA, left/right VA) were parallel to each other. While this position allows the arteries to be “capture” in one PC scan, it has three pitfalls. First, any arterial branching (or even merging) between this location and the foramen magnum, where the

arteries enter the skull, could result in bias in CBF estimation. Second, the level of C3 is more distant from the iso-center of the magnet, thus the actual gradient strength experienced by the blood spins may be lower than nominal values, resulting in under-estimation in flow velocity. Finally, in some individuals, the common carotid artery has not branched at this level, thus the estimated flow may include both internal and external carotids. Therefore, in the present study, we acquired PC MRI at a higher location immediately adjacent to foramen magnum using four separate scans. The additional time needed for extra PC scans was offset by the time saved from the TRUST scan. Thus the total time was still within 5 minutes.

We observed that CBF and OEF co-varied across sessions and across subjects, and as a result the variations in $CMRO_2$, the product of CBF and OEF, were actually smaller than those of the individual factors. That is, although vascular parameters (blood flow and blood oxygenation) show large inter-subject variations due to numerous physiologic reasons (e.g. breathing pattern, blood pressure, consumption of caffeine), the brain's metabolic rate does not show much variability across days or across individuals of similar age, making this parameter an excellent biomarker for studies of diseased conditions.

Compared to the calibrated fMRI technique, the $CMRO_2$ method used in the present study does not require the use of inhalation tasks such as hypercapnia or hyperoxia (24–26,28) and the measurement duration is relatively short. In fact, the proposed method may be applied to physiologic challenges to test certain assumptions made in the calibrated fMRI method (e.g. hypercapnia and hyperoxia do not alter $CMRO_2$) (35–36). On the other hand, the advantage of calibrated fMRI is that this technique provides a potential to map $CMRO_2$ on a region-by-region basis (28).

The main limitation of the present $CMRO_2$ technique is its lack of spatial resolution. The evaluations of Y_v, CBF and $CMRO_2$ were all based on global measures. Since this technique cannot provide regional $CMRO_2$ information, this technique will have limited utility in brain diseases with focal or inhomogeneous metabolic changes, such as acute stroke and brain tumor, unless the lesion regions cover the majority of the brain. However, global $CMRO_2$ may find applications in certain clinical scenarios, especially given that the technique can be completed within 5 minutes with a small CoV of 4% using completely non-invasive procedures on a standard 3T system. We have previously demonstrated the utility of this technique in cognitive aging (4), multiple sclerosis (5), and CO_2 modulation of brain metabolism (35). This technique can also be applied to other pathological conditions. In particular, the present technique may be of great benefit in studies of brain development in children including neonates, in whom the use of radioactively labeled tracers may not be justifiable.

A physiologic confound of the present technique is hematocrit. The hematocrit level may affect the estimated $CMRO_2$ value by two means. One is that the relationship between blood T_2 and oxygenation is dependent on hematocrit and thus, for the same measured T_2, the actual oxygenation could be slightly different for different hematocrit. A second effect is that the value of C_a in Eq. [1] is expected to be proportional to hematocrit because the oxygen carrying capacity will be greater if there is more hemoglobin in the blood. Fortunately, these two confounding effects of hematocrit have opposite consequences on $CMRO_2$, thus they partially cancel out. Our earlier simulation study showed that, within normal hematocrit range of 0.38 to 0.50, the bias in the estimated $CMRO_2$ was −5.6% to 7.1% of the true value (21). However, for conditions where hematocrit may be substantially out of normal range (e.g. anemia), a blood sample should be obtained and a hematocrit-specific blood calibration curve (40) and C_a should be used in the calculation of $CMRO_2$. Similarly, in conditions where red blood cell or hemoglobin is different (e.g. sickle cell

disease (48), fetal hemoglobin in neonate applications (49), new blood calibration curves should be obtained for accurate estimation of $CMRO_2$.

Conclusion

Intra-session and inter-session variability of the proposed $CMRO_2$ procedure is comparable or slightly smaller than that using ^{15}O PET. Inter-subject variations in $CMRO_2$ were found to be smaller than that of the vascular parameters, CBF and OEF. Its simplicity and reliability features may afford this technique great potential for immediate clinical applications.

Acknowledgments

Grant Sponsors: NIH R01 MH084021, NIH R01 NS067015, NIH R21 AG034318, NIH R01 AG033106

REFERENCES

1. Magistretti PJ, Pellerin L. Cellular mechanisms of brain energy metabolism and their relevance to functional brain imaging. Philos Trans R Soc Lond B Biol Sci. 1999; 354(1387):1155–1163. [PubMed: 10466143]
2. Buckner RL, Snyder AZ, Shannon BJ, LaRossa G, Sachs R, Fotenos AF, Sheline YI, Klunk WE, Mathis CA, Morris JC, Mintun MA. Molecular, structural, and functional characterization of Alzheimer's disease: evidence for a relationship between default activity, amyloid, and memory. J Neurosci. 2005; 25(34):7709–7717. [PubMed: 16120771]
3. Ogawa M, Fukuyama H, Ouchi Y, Yamauchi H, Kimura J. Altered energy metabolism in Alzheimer's disease. J Neurol Sci. 1996; 139(1):78–82. [PubMed: 8836976]
4. Lu H, Xu F, Rodrigue KM, Kennedy KM, Cheng Y, Flicker B, Hebrank AC, Uh J, Park DC. Alterations in cerebral metabolic rate and blood supply across the adult lifespan. Cereb Cortex. 2011; 21(6):1426–1434. [PubMed: 21051551]
5. Ge Y, Zhang Z, Lu H, Tang L, Jaggi H, Herbert J, Babb JS, Rusinek H, Grossman RI. Characterizing brain oxygen metabolism in patients with multiple sclerosis with T2-relaxation-under-spin-tagging MRI. J Cereb Blood Flow Metab. 2012 DOI: 10.1038/jcbfm.2011.191.
6. Sun X, Tanaka M, Kondo S, Okamoto K, Hirai S. Clinical significance of reduced cerebral metabolism in multiple sclerosis: a combined PET and MRI study. Ann Nucl Med. 1998; 12(2):89–94. [PubMed: 9637279]
7. Borghammer P, Vafaee M, Ostergaard K, Rodell A, Bailey C, Cumming P. Effect of memantine on CBF and CMRO2 in patients with early Parkinson's disease. Acta Neurol Scand. 2008; 117(5):317–323. [PubMed: 17927800]
8. Sieber FE, Brown PR, Wu Y, Koehler RC, Traystman RJ. Cerebral blood flow and metabolism in dogs with chronic diabetes. Anesthesiology. 1993; 79(5):1013–1021. [PubMed: 8238980]
9. Uchino K, Lin R, Zaidi SF, Kuwabara H, Sashin D, Bircher N, Chang YF, Hammer MD, Reddy V, Jovin TG, Vora N, Jumaa M, Massaro L, Billigen J, Boada F, Yonas H, Nemoto EM. Increased Cerebral Oxygen Metabolism and Ischemic Stress in Subjects with Metabolic Syndrome-Associated Risk Factors: Preliminary Observations. Transl Stroke Res. 2010; 1(3):178–183. [PubMed: 22034586]
10. Glenn TC, Kelly DF, Boscardin WJ, McArthur DL, Vespa P, Oertel M, Hovda DA, Bergsneider M, Hillered L, Martin NA. Energy dysfunction as a predictor of outcome after moderate or severe head injury: indices of oxygen, glucose, and lactate metabolism. J Cereb Blood Flow Metab. 2003; 23(10):1239–1250. [PubMed: 14526234]
11. Walter C, Hertel F, Naumann E, Morsdorf M. Alteration of cerebral perfusion in patients with idiopathic normal pressure hydrocephalus measured by 3D perfusion weighted magnetic resonance imaging. J Neurol. 2005; 252(12):1465–1471. [PubMed: 16021357]
12. Bremmer JP, van Berckel BN, Persoon S, Kappelle LJ, Lammertsma AA, Kloet R, Luurtsema G, Rijbroek A, Klijn CJ, Boellaard R. Day-to-day test-retest variability of CBF, CMRO2, and OEF

measurements using dynamic 15O PET studies. Mol Imaging Biol. 2011; 13(4):759–768. [PubMed: 20700768]

13. Coles JP, Fryer TD, Bradley PG, Nortje J, Smielewski P, Rice K, Clark JC, Pickard JD, Menon DK. Intersubject variability and reproducibility of 15O PET studies. J Cereb Blood Flow Metab. 2006; 26(1):48–57. [PubMed: 15988475]
14. Fox PT, Raichle ME. Focal physiological uncoupling of cerebral blood flow and oxidative metabolism during somatosensory stimulation in human subjects. Proc Natl Acad Sci U S A. 1986; 83(4):1140–1144. [PubMed: 3485282]
15. Mintun MA, Raichle ME, Martin WR, Herscovitch P. Brain oxygen utilization measured with O-15 radiotracers and positron emission tomography. J Nucl Med. 1984; 25(2):177–187. [PubMed: 6610032]
16. Zhu XH, Zhang Y, Tian RX, Lei H, Zhang N, Zhang X, Merkle H, Ugurbil K, Chen W. Development of (17)O NMR approach for fast imaging of cerebral metabolic rate of oxygen in rat brain at high field. Proc Natl Acad Sci U S A. 2002; 99(20):13194–13199. [PubMed: 12242341]
17. Kety SS, Schmidt CF. The effects of altered arterial tensions of carbon dioxide and oxygen on cerebral blood flow and cerebral oxygen consumption of normal young men. J Clin Invest. 1948; 27(4):484–492. [PubMed: 16695569]
18. Taudorf S, Berg RM, Bailey DM, Moller K. Cerebral blood flow and oxygen metabolism measured with the Kety-Schmidt method using nitrous oxide. Acta Anaesthesiol Scand. 2009; 53(2):159–167. [PubMed: 19076112]
19. Hyder F, Chase JR, Behar KL, Mason GF, Siddeek M, Rothman DL, Shulman RG. Increased tricarboxylic acid cycle flux in rat brain during forepaw stimulation detected with 1H[13C]NMR. Proc Natl Acad Sci U S A. 1996; 93(15):7612–7617. [PubMed: 8755523]
20. An H, Lin W, Celik A, Lee YZ. Quantitative measurements of cerebral metabolic rate of oxygen utilization using MRI: a volunteer study. NMR Biomed. 2001; 14(7–8):441–447. [PubMed: 11746936]
21. Xu F, Ge Y, Lu H. Noninvasive quantification of whole-brain cerebral metabolic rate of oxygen (CMRO2) by MRI. Magn Reson Med. 2009; 62(1):141–148. [PubMed: 19353674]
22. Chen JJ, Pike GB. Global cerebral oxidative metabolism during hypercapnia and hypocapnia in humans: implications for BOLD fMRI. J Cereb Blood Flow Metab. 2010; 30(6):1094–1099. [PubMed: 20372169]
23. Elwell CE, Henty JR, Leung TS, Austin T, Meek JH, Delpy DT, Wyatt JS. Measurement of CMRO2 in neonates undergoing intensive care using near infrared spectroscopy. Adv Exp Med Biol. 2005; 566:263–268. [PubMed: 16594161]
24. Davis TL, Kwong KK, Weisskoff RM, Rosen BR. Calibrated functional MRI: mapping the dynamics of oxidative metabolism. Proc Natl Acad Sci U S A. 1998; 95(4):1834–1839. [PubMed: 9465103]
25. Hoge RD, Atkinson J, Gill B, Crelier GR, Marrett S, Pike GB. Investigation of BOLD signal dependence on cerebral blood flow and oxygen consumption: the deoxyhemoglobin dilution model. Magn Reson Med. 1999; 42(5):849–863. [PubMed: 10542343]
26. Chiarelli PA, Bulte DP, Gallichan D, Piechnik SK, Wise R, Jezzard P. Flow-metabolism coupling in human visual, motor, and supplementary motor areas assessed by magnetic resonance imaging. Magn Reson Med. 2007; 57(3):538–547. [PubMed: 17326178]
27. Leontiev O, Buxton RB. Reproducibility of BOLD, perfusion, and CMRO2 measurements with calibrated-BOLD fMRI. Neuroimage. 2007; 35(1):175–184. [PubMed: 17208013]
28. Gauthier CJ, Hoge RD. Magnetic resonance imaging of resting OEF and CMRO(2) using a generalized calibration model for hypercapnia and hyperoxia. Neuroimage. 2012; 60(2):1212–1225. [PubMed: 22227047]
29. He X, Yablonskiy DA. Quantitative BOLD: mapping of human cerebral deoxygenated blood volume and oxygen extraction fraction: default state. Magn Reson Med. 2007; 57(1):115–126. [PubMed: 17191227]
30. Jain V, Langham MC, Wehrli FW. MRI estimation of global brain oxygen consumption rate. J Cereb Blood Flow Metab. 2010; 30(9):1598–1607. [PubMed: 20407465]

31. Brown DW, Hadway J, Lee TY. Near-infrared spectroscopy measurement of oxygen extraction fraction and cerebral metabolic rate of oxygen in newborn piglets. Pediatr Res. 2003; 54(6):861–867. [PubMed: 12930911]
32. Tichauer KM, Elliott JT, Hadway JA, Lee DS, Lee TY, St Lawrence K. Using near-infrared spectroscopy to measure cerebral metabolic rate of oxygen under multiple levels of arterial oxygenation in piglets. J Appl Physiol. 2010; 109(3):878–885. [PubMed: 20616228]
33. Haccke, EM.; Brown, RW.; Thompson, MR.; Venkatesan, R. Magnetic Resonance Imaging: Physical Principles and Sequence Design. Wiley-Liss; New York, NY: 1999. MR Angiography and Flow Quantification.
34. Lu H, Ge Y. Quantitative evaluation of oxygenation in venous vessels using T2-Relaxation-Under-Spin-Tagging MRI. Magn Reson Med. 2008; 60(2):357–363. [PubMed: 18666116]
35. Xu F, Uh J, Brier MR, Hart J Jr. Yezhuvath US, Gu H, Yang Y, Lu H. The influence of carbon dioxide on brain activity and metabolism in conscious humans. J Cereb Blood Flow Metab. 2011; 31(1):58–67. [PubMed: 20842164]
36. Xu, F.; Liu, P.; Lu, H. Effect of graded O2 challenge on vascular and metabolic parameters. Proceedings of the 19th Annual Meeting of ISMRM; Montreal, Canada. 2011. p. 253
37. Xu, F.; Liu, P.; Lu, H. Acute and chronic effects of glucose on brain metabolism: findings from healthy subjects and diseased conditions. Proceedings of the 20th Annual Meeting of ISMRM; Melborne, Australia. 2012. p. 2915
38. Xu F, Uh J, Liu P, Lu H. On improving the speed and reliability of T(2) - relaxation-under-spin-tagging (TRUST) MRI. Magn Reson Med. 2011 DOI: 10.1002/mrm.23207.
39. Guyton, AC.; Hall, JE. Respiration. In: Guyton, AC.; Hall, JE., editors. Textbook of medical physiology. 11th ed.. Saunders/Elsevier; Philadelphia: 2005.
40. Lu H, Xu F, Grgac K, Liu P, Qin Q, van Zijl P. Calibration and validation of TRUST MRI for the estimation of cerebral blood oxygenation. Magn Reson Med. 2012; 67(1):42–49. [PubMed: 21590721]
41. Bakker CJ, Hoogeveen RM, Viergever MA. Construction of a protocol for measuring blood flow by two-dimensional phase-contrast MRA. J Magn Reson Imaging. 1999; 9(1):119–127. [PubMed: 10030659]
42. Evans AJ, Iwai F, Grist TA, Sostman HD, Hedlund LW, Spritzer CE, Negro-Vilar R, Beam CA, Pelc NJ. Magnetic resonance imaging of blood flow with a phase subtraction technique. In vitro and in vivo validation. Invest Radiol. 1993; 28(2):109–115. [PubMed: 8444566]
43. Zananiri FV, Jackson PC, Goddard PR, Davies ER, Wells PN. An evaluation of the accuracy of flow measurements using magnetic resonance imaging (MRI). J Med Eng Technol. 1991; 15(4–5): 170–176. [PubMed: 1800748]
44. Chen Y, Wang DJ, Detre JA. Test-retest reliability of arterial spin labeling with common labeling strategies. J Magn Reson Imaging. 2011; 33(4):940–949. [PubMed: 21448961]
45. Golay X, Hendrikse J, Lim TC. Perfusion imaging using arterial spin labeling. Top Magn Reson Imaging. 2004; 15(1):10–27. [PubMed: 15057170]
46. Yang Y, Engelien W, Xu S, Gu H, Silbersweig DA, Stern E. Transit time, trailing time, and cerebral blood flow during brain activation: measurement using multislice, pulsed spin-labeling perfusion imaging. Magn Reson Med. 2000; 44(5):680–685. [PubMed: 11064401]
47. Bolar DS, Rosen BR, Sorensen AG, Adalsteinsson E. Quantitative Imaging of extraction of oxygen and TIssue consumption (QUIXOTIC) using venular-targeted velocity-selective spin labeling. Magn Reson Med. 2011; 66(6):1550–1562. [PubMed: 21674615]
48. Serjeant, GR.; Serjeant, BE. Sickle cell disease. Oxford University Press; Oxford: 2001.
49. Zijlstra WG, Buursma A, Meeuwsen-van der Roest WP. Absorption spectra of human fetal and adult oxyhemoglobin, de-oxyhemoglobin, carboxyhemoglobin, and methemoglobin. Clin Chem. 1991; 37(9):1633–1638. [PubMed: 1716537]

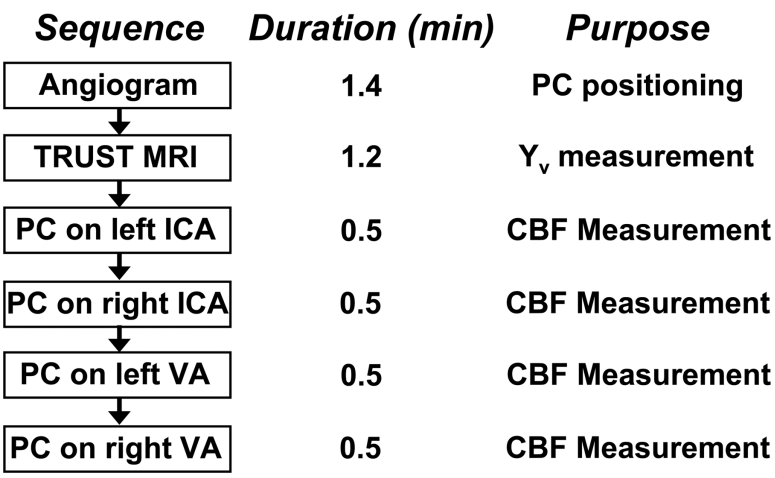

Fig. 1.
Proposed MRI procedure for a complete $CMRO_2$ dataset.

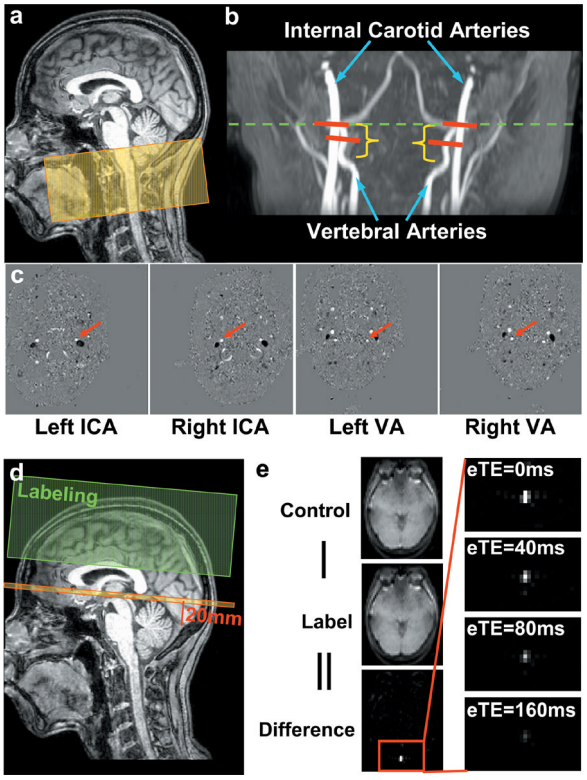

Fig. 2.

Illustration of the positions of the MRI scans and representative images. (a) Slice position of the 3D angiogram scan that is needed to visualize the feeding arteries. (b) Typical results of the angiogram scan with slice positions of the PC MRI scans. The four PC MRI scans (red bars) are positioned perpendicular to the respective feeding arteries based on the MIP image of the angiogram. The green dash line indicates the level of foramen magnum where the arteries enter the skull. The corresponding phase images from the PC MRI scans are shown in (c). The targeted arteries are pointed out by the red arrows. (d) Imaging slice (yellow) and labeling slab (green) of the TRUST MRI scan. The imaging slice was positioned to be parallel to anterior-commissure posterior-commissure line with a distance of 20 mm from the sinus congruence. (e) Typical data of TRUST MRI. The subtraction of the control and labeled images yields blood signal, which is then subject to increasing T_2 weightings. Monoexponential fitting of the signal as a function of eTE results in T_2 estimation.

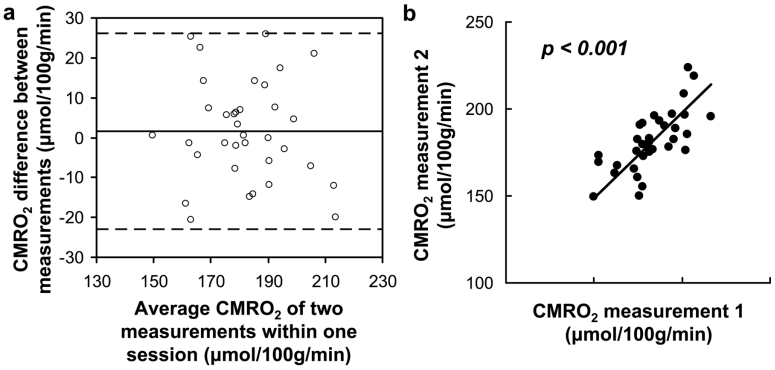

Fig. 3.

Intra-session reproducibility of the $CMRO_2$ measurements. (a) Bland–Altman plot comparing two $CMRO_2$ measurements obtained within one session. The solid line indicates the mean difference between two measurements. The dashed lines indicate the 95% confidence interval. (b) Scatter plot of the two $CMRO_2$ measurements. Each dot represents data from one session of one subject. The solid line indicates the linear regression curve (r = 0.67, $p < 0.0001$).

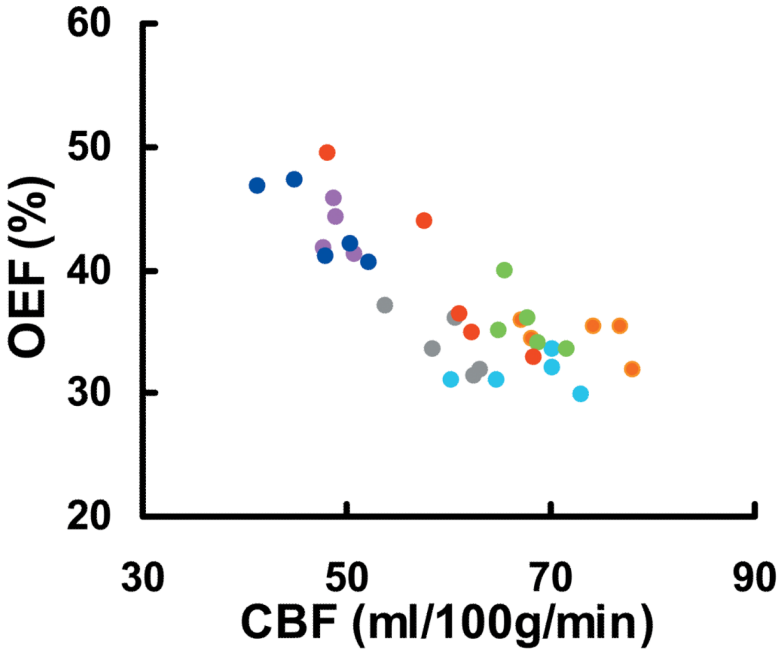

Fig. 4.

Scatter plot of CBF and OEF measurements across subjects and across sessions. Each dot represents data from one session of one subject. Different sessions from one subject are shown in the same color. CBF and OEF are correlated across sessions ($p = 0.002$ from Mixed Effect Model analysis) and across subjects ($p = 0.01$ from Pearson correlation).

Table 1

Summary of the intra-session, inter-session, and inter-subject CoV (Mean ± SD, N=7).

	Y_v	OEF	CBF	$CMRO_2$
Mean ± SD	61.73 ± 4.62 (%)	37.50 ± 4.83 (%)	60.57 ± 9.70 (ml/100g/min)	182.25 ± 11.97 (μmol/100g/min)
Intra-session variability:				
CoV (%)	1.88 ± 0.57	3.19 ± 1.20	2.77 ± 0.82	3.84 ± 1.44
Inter-session variability:				
CoV (%)	5.06 ± 3.12	8.16 ± 4.46	7.41 ± 2.99	6.59 ± 1.56
Inter-subject variability:				
CoV (%)	9.15	15.61	17.40	8.80